N- and P-Channel Transport Behavior in Thin Film Transistors Based on Tricyanovinyl-Capped Oligothiophenes

Xiuyu Cai,[†] Michael W. Burand,[‡] Christopher R. Newman,[†] Demetrio A. da Silva Filho,[§] Ted M. Pappenfus,[||] Mamoun M. Bader,[⊥] Jean-Luc Brédas,[§] Kent R. Mann,[‡] and C. Daniel Frisbie*,[†]

Department of Chemical Engineering and Materials Science, University of Minnesota, 421 Washington Avenue SE, Minneapolis, Minnesota 55455, Department of Chemistry, University of Minnesota, 207 Pleasant Street SE, Minneapolis, Minnesota 55455, School of Chemistry and Biochemistry, Georgia Institute of Technology, Atlanta, Georgia 30332, Division of Science and Mathematics, University of Minnesota, Morris, Minnesota 56267, and Chemistry Department, Pennsylvania State University, Hazleton, Pennsylvania 18202

Received: February 23, 2006; In Final Form: May 23, 2006

We report the structural and electrical characterization of thin films of organic semiconductor molecules consisting of an oligothiophene core capped with electron-withdrawing tricyanovinyl (TCV) groups. X-ray diffraction and atomic force microscopy of evaporated films of three different TCV-capped oligothiophenes showed that the films were highly crystalline. Electrical transport was measured in thin film transistors employing silver source and drain contacts and channel probes to correct for contact resistance. Three compounds exhibited n-channel (electron) conduction consistent with cyclic voltametry data that indicated they undergo facile reduction. Maximum electron mobilities were 0.02 $cm^2/V \cdot s$ with an on/off current ratio of 10^6. A fourth end-capped molecule, TCV-6T-TCV, which had six thiophene rings, exhibited both p- and n-channel transport. Overall, these results confirm that substitution of oligothiophene cores with electron-withdrawing groups is a useful strategy to achieve electron-transporting materials.

1. Introduction

Thiophene-based organic semiconductors have been extensively investigated for organic thin film transistor (OTFT) applications due to their high mobility and stability.[1−10] The electronic properties of these molecules have been modified through the introduction of different chemical substituents. In most OTFTs, oligothiophenes function as p-channel (hole-conducting) semiconductors,[11−14] although recent work has shown that oligothiophenes substituted with electron-withdrawing groups can be n-channel (electron) conductors in OTFTs.[15] Modifying p-channel oligothiophene cores with strongly electronegative substituents may lower LUMO energies and facilitate electron injection, thus changing the semiconductor from a hole to an electron conductor. Recently, perfluorohexyl-,[3,9,16,17] perfluoroarene-,[18] carbonyl-,[19] and dicyanomethyl-[20,21] modified oligothiophenes have been synthesized and proven to be good n-channel organic semiconductors. Moreover, several groups have synthesized tricyanovinyl-substituted oligothiophenes (TCVTs) with tricyanovinyl (TCV) electron-withdrawing groups,[22,23] but these were not tested in OTFTs. The electrochemical data for these compounds show that, in addition to the oxidation peaks intrinsic for oligothiophenes, reduction peaks are also present at relatively modest potentials, suggesting that facile injection of electrons into TCVT films should be possible. In addition, CN---H hydrogen-bonding interactions allow close intermolecular packing,[24] which should promote efficient charge carrier transport.

Facchetti et al.[17,18] found that regiochemistry, i.e., relative building-block connectivity, determines the majority carrier sign for perfluoroarene-modified polythiophene and fluorocarbon-substituted sexithiophenes. Movement of the fluorinated moiety from the molecular periphery to the core inverted the majority carrier from electrons to holes. This phenomenon was rationalized as being a consequence of the charge injection properties of the metal−organic interface (i.e., the contacts),[17] molecular electronic structure, and screening of environmental traps.[18] Differences in the properties of the semiconductor−insulator interface might also be important in determining the mobile carrier sign.

In this paper, we present a series of new n-channel organic semiconductors based on oligothiophenes with tricyanovinyl electron-withdrawing groups, shown in Scheme 1. The observed electronic properties demonstrate that n-channel organic semiconductors with tricyanovinyl-modified p-channel cores may be developed. Increasing the conjugation length of the thiophene core changed the majority carriers from electrons to holes. In the longest TCV-substituted oligomer, we observe ambipolar (p- and n-channel) transport.

2. Experimental Methods

2.A. Synthesis. All syntheses were carried out using oven-dried glassware. Tetrahydrofuran was distilled from Na/benzophenone under N_2 for the synthesis of **2** and was dried via an MBraun SPS for the other syntheses. Tertracyanoethylene (Aldrich) was recrystallized from 1,2-dichloroethane prior to the synthesis of **2**. *N*-Butyllithium (2.5 M solution in hexanes) (Aldrich) was used as received. 3,3″-Dihexyl-2,2′:5′,2″-terthiophene and 3,3‴-dihexyl-2,2′:5′,2″:5″,2‴-quaterthiophene

* Corresponding author. E-mail: frisbie@cems.umn.edu.
[†] Department of Chemical Engineering and Materials Science, University of Minnesota.
[‡] Department of Chemistry, University of Minnesota.
[§] Georgia Institute of Technology.
[||] Division of Science and Mathematics, University of Minnesota.
[⊥] Pennsylvania State University.

10.1021/jp061168v CCC: $33.50
Published on Web 07/13/2006

SCHEME 1: Chemical Structures of Tricyanovinyl-Capped Oligothiophenes 1−4

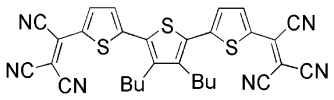

1

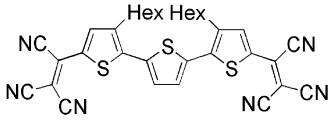

2

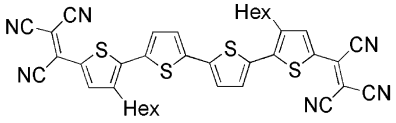

3

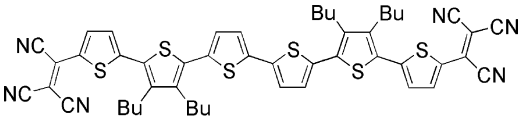

4

were available from a previous study.[25] Compounds **1** and **4** were prepared as described previously.[23] ^{1}H NMR spectra were measured on a Varian Inova (300 MHz) instrument. The chemical shifts are reported in ppm and the coupling constants (*J*) are given in Hz. All spectra are referenced to the residual proton peak of the chloroform solvent, 7.27 ppm. Mass spectra were obtained on a Finnigan MAT 95 mass spectrometer. Solution electronic spectra in dichloromethane solutions were collected on an Ocean Optics spectrophotometer. Electrochemical experiments were performed with a BAS 100B electrochemical analyzer and a glassy carbon working electrode. Solutions of electroactive compound (∼0.5 mM) were made in dichloromethane with 0.1 M $TBAPF_6$ as the supporting electrolyte. Potentials are reported vs aqueous Ag/AgCl and are not corrected for the junction potential. The $E^{\circ\prime}$ value for the ferrocenium/ferrocene couple under the conditions used in this study was +0.46 V.[26]

*2.A.1. Synthesis of **2**. 3,3″-Dihexyl-5,5″-bis(tricyanovinyl)-2,2′:5′,2″-terthiophene (**2**).* To a 100 mL Schlenk flask were added 3,3″-dihexyl-2,2′:5′,2″-terthiophene (1.00 g, 2.40 mmol) and tertrahydrofuran (45 mL) at −78 °C under Ar. To this solution was added *n*-butyllithium (2.5 M in hexanes) (2.02 mL, 5.05 mmol) dropwise over a period of 15 min. The resulting solution was warmed to 0 °C for 5 min and then cooled to −78 °C. Tetracyanoethylene (750 mg, 5.86 mmol) was added in one portion, and the solution was allowed to stir for 35 min. The solution was warmed to room temperature and water (20 mL) was added. The solvent was removed by rotary evaporation, and the resulting mixture was filtered through diatomaceous earth. The diatomaceous earth was extracted with dichloromethane (300 mL) and filtered through paper. The solution volume was decreased to approximately 20 mL by rotary evaporation and then filtered on a short pad of silica gel. Further purification was achieved via column chromatography on silica gel, first eluted with a 2:1 mixture of dichloromethane:hexanes, followed by elution with 100% dichloromethane. This yielded 58.7 mg (4%) of **2** as a metallic purple solid. ^{1}H NMR (300 MHz, $CDCl_3$): δ 7.92 (s, 2H), 7.50 (s, 2H), 2.89 (t, 4H, J = 7.8), 1.80−1.25 (m), 0.91 (t, J = 6.9). UV−vis (CH_2Cl_2, nm): 567. HREIMS calcd, 618.1694; found 618.1739 (M^+).

*2.A.2. Synthesis of **3**. 3,3‴-Dihexyl-5,5‴-bis(tricyanovinyl)-2,2′:5′,2″:5″,2‴-quaterthiophene (**3**).* To a 50 mL Schlenk flask were added 3,3‴-dihexyl-2,2′:5′,2″:5″,2‴-quaterthiophene (318 mg, 0.637 mmol) and tertrahydrofuran (20 mL) at −78 °C under Ar. To this solution was added *n*-butyllithium (2.5 M in hexanes) (0.54 mL, 1.35 mmol) dropwise over a period of 15 min. The resulting solution was warmed to 0 °C for 5 min and then cooled to −78 °C. Tetracyanoethylene (200 mg, 1.56 mmol) was added in one portion, and the solution was allowed to stir for 10 min. The solution was allowed to warm to room temperature and stirred for 1 h, and then water (10 mL) was added. The solvent was removed by rotary evaporation, and the resulting solid was dissolved in dichloromethane and dried with $MgSO_4$. Purification was achieved via column chromatography on silica gel with 100% chloroform. This yielded 38 mg (9%) of **3** as a copper-colored solid. ^{1}H NMR (300 MHz, $CDCl_3$): δ 7.89 (s, 2H), 7.45 (d, 2H, J = 3.9), 7.35 (d, 2H, J = 4.2), 2.89 (t, 4H, J = 7.8), 1.80−1.25 (m), 0.92 (t, J = 6.9). UV−vis (CH_2Cl_2, nm): 610. HREIMS calcd, 700.1566; found, 700.1551 (M^+).

2.B. Film Growth and Characterization. Thin films of the compounds were prepared by thermal evaporation from an alumina crucible placed in a Radak I furnace with feedback temperature control onto a resistively heated and water-cooled copper block. The base pressure was approximately 4×10^{-7} Torr. After multiple sublimations, no visible degradation of the source materials was observed, indicating that these molecules are thermally stable. Film thickness was measured by a quartz crystal monitor, which was calibrated using thickness values obtained by atomic force microscopy (AFM) on as-deposited films. The growth rate was held at 0.02 Å/s for the initial 60 Å and then increased to 0.1 Å/s for a total thickness of 350 Å.

The structure and crystallinity of the thin films were characterized by wide-angle X-ray diffraction using a Philips X'Pert system with a Cu Kα_1 (λ = 1.5406 Å) source. Standard $\theta-2\theta$ scans were obtained from 2 to 18° (2θ) with a dwell time of 1 s per step. Powder diffraction patterns of these four compounds were obtained by the same instrument with a dwell time of 1.5 s per step.

Thin film morphology was examined using atomic force microscopy. A Digital Instruments Dimension 3100 AFM was used in tapping mode with Si cantilevers (MicroMasch) and all images were taken in air.

2.C. Substrate Preparation and Device Fabrication. Heavily doped p-type silicon wafers (Silicon Valley Microelectronics) with 3000 Å thermally grown silicon dioxide were used as substrates for device fabrication. After removal of the SiO_2 from the backside, 100 Å aluminum and 750 Å gold were deposited by e-beam evaporation followed by rapid thermal annealing at 450 °C to form an ohmic contact to silicon. These hydrophilic substrates are referred to as bare SiO_2 in this paper. Hydrophobic substrates (PS−SiO_2 and HMDS−SiO_2) were prepared by spin-coating a thin layer (∼100 Å) of 680 kg/mol poly(α-methyl styrene) onto SiO_2 substrates according to the patent published by 3M Company or by exposing the bare SiO_2 substrates to saturated hexamethyldisilazane (HMDS) vapor for several minutes. Al_2O_3 substrates were chemically mechanically polished (CMP) to a RMS roughness equivalent to thermally grown SiO_2. CMP was performed by Polishing Solutions International, LLC, Tempe, AZ. Hydrophobic C_{16}-alkane chain terminated Al_2O_3 substrates were fabricated by the published procedure and will be called $C_{16}-Al_2O_3$.

Organic semiconductor thin films (350 Å) were deposited on the substrates described above through stainless steel shadow masks, which defined the area of the organic thin film to reduce

parasitic leak. Source, drain, and voltage sensing electrodes (to correct for contact effects) were deposited by thermal evaporation of 400 Å Ag through a pre-aligned silicon shadow mask. The transistor channel width (W) was 2000 μm and length (L) 200 μm. Voltage sensing electrodes ($\sim$10 μm width) were located at (1/3)L and (2/3)L and penetrated the channel 125 μm.

2.D. Electrical Characterization. Electrical characterization was performed in the dark using a Desert Cryogenics probe station with a base pressure of 5×10^{-7} Torr. Variable temperature measurements were conducted over the temperature range 145−315 K with a 10 K decrease step. Source and drain voltages were applied with a Keithley 236 and Keithley 237 source measure unit, respectively. Gate voltages were applied with a Keithley 6517A electrometer. Channel voltages were sensed with Keithley 6517A electrometers. All units have an impedance of 10^{14} Ω.

Linear mobilities were calculated using the four-probe technique by eq 1,

$$\mu = \frac{L_{\text{channel}}}{WC_{\text{i}}} \frac{\mathrm{d}(I_{\text{D}}/V_{12})}{\mathrm{d}V_{\text{G12}}} \tag{1}$$

where W is the channel width, C_{i} is the capacitance of the insulator, $L_{\text{channel}} = L_2 - L_1$, $V_{12} = V_2 - V_1$, and $V_{\text{G12}} = V_{\text{G}} - (V_1 + V_2)/2$; here V_1 and V_2 are the voltages measured by the sensing probes. The turn-on voltage (V_0) was defined as the onset of exponential current increase from a logarithmic plot of drain current (log I_{D}) versus gate voltage (V_{G}). The $I_{\text{D}} - V_{\text{G}}$ sweeps were taken from −10 to 30 V with a step size of 0.5 V and a delay time of 0.5 s between each step for devices on alumina substrates and from −50 to 100 V with a step size of 1 V and a delay time of 0.5 s for devices on silica substrates.

2.E. Electronic Structure Calculation. We performed geometry optimizations for the neutral state of **1** and **4** followed by the analysis of the frontier molecular orbitals. The calculations were carried out at the density functional theory (DFT) level using the B3LYP functional, involving the three-parameter exchange functional of Becke,[27,28] and the correlation functional of Lee, Yang, and Parr,[29] as implemented in Gaussian03.[30] A split-valence plus polarization 6-31G**[31−35] basis set was used in all calculations. For simplicity, the C_6H_{13} and C_4H_9 groups have been replaced by C_2H_5 in the calculations since the electronic structure of isolated molecules in the region of interest is hardly influenced by long aliphatic chains.

3. Results and Discussion

3.A. Synthesis. Compounds **2** and **3** were prepared by synthetic routes similar to those reported for analogous molecules.[23,36−38] The precursor oligothiophene is dilithiated at low temperature, and the resulting dianion is treated with tetracyanoethylene to afford the tricyanovinyl-capped product. Purification of these compounds required extensive column chromatography, and the products were obtained in only modest yields. Yields may be improved by modifications of synthetic procedures as we have recently described.[39]

3.B. Electrochemistry. Solution electrochemical data show reversible oxidation and reduction processes for compounds **1**−**4** (Figure 1). All the compounds in this study undergo two two-electron reductions. The potentials at which these reductions occur vary little from one compound to the next. The first reduction process is shifted to slightly more negative potentials with an increase in the number of thiophene rings, whereas the second reduction is shifted to a slightly more positive value. Conversely, compounds **1**−**4** become significantly easier to oxidize with an increase in the number of thiophene rings. In the case of oligomers **3** and **4**, a second, reversible oxidation process is observed. These data are summarized in Table 1. This indicates that the oxidation processes in TCV-capped oligothiophenes, such as the ones presented in this study, may be electronically tuned by varying the number of thiophene rings in the oligomer chain.

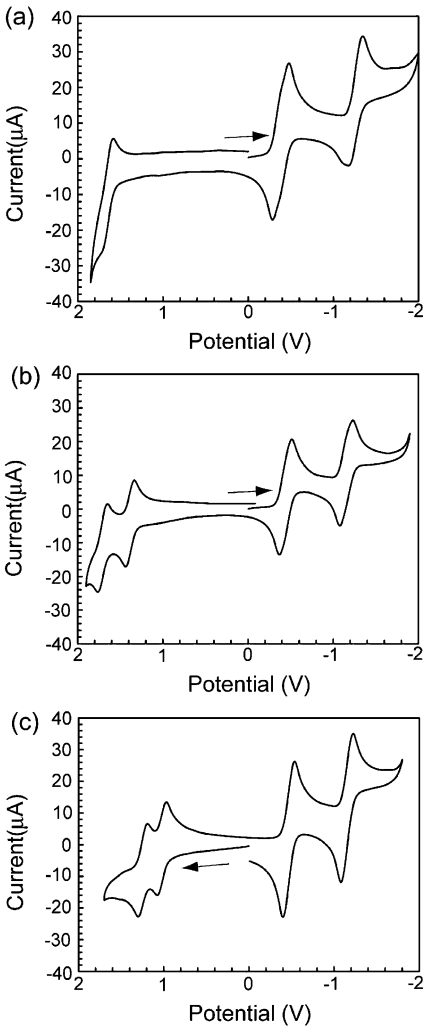

Figure 1. Cyclic voltammograms of **1**,[23] **3**, and **4**[23] in 0.1 M $TBAPF_6$/CH_2Cl_2, ν = 100 mV/s, with an Ag/AgCl reference electrode.

3.C. Electronic Structure. The HOMO and LUMO energies for tricyanovinyl (TCV), terthiophene (T_3), sexithiophene (T_6), **1** and **4** are displayed in Figure 2. As expected, with extension of the thiophene segment from terthienyl to sexithienyl, the band gap reduces with the HOMO being destabilized and the LUMO stabilized. This stabilization energy is, however, small with respect to the difference in energy of these orbitals in TCV vs the oligothiophene subunits. With a simple comparison of the orbital energies of the fragments, it is expected that **1**/**4** HOMO is mainly constituted by the T_3/T_6 HOMO while the LUMO mainly originates in the TCV subunit.

Figure 3 displays the HOMO and LUMO orbitals of **1** and **4**. The different degree of (de)localization of these orbitals can be rationalized in terms of the electronic coupling between the two TCV units. This coupling is inversely proportional to the distance between the two TCV groups. The shorter the distance between the two units, the larger will be the coupling and thus the delocalization of the molecular orbital. In the case of **1**, the two TCV groups are closer than those in **4** and thus the

TABLE 1: Electronic Properties of All the Compounds Obtained Both from Transistors and Electrochemical Cells

	transistor data				electrochemical data	
oligomer	substrate	μ ($cm^2/V\cdot s$) and type	V_T (V)	$I_{on/off}$	oxidation process $E°$ (V)	reduction process[a] $E°$ (V)
1	$C_{16}-Al_2O_3$	0.02 (n)	9.4	10^6	1.72	−0.36 ($n = 2$)
	bare SiO_2	2.8×10^{-4} (n)	8	3.2×10^5		−1.33 ($n = 2$)
2	HMDS−SiO_2	2.0×10^{-3} (n)	4	1.4×10^7	1.67	−0.38 ($n = 2$)
	bare SiO_2	2.5×10^{-4} (n)	4	1.1×10^6		−1.27 ($n = 2$)
3	HMDS−SiO_2	9.2×10^{-4} (n)	14	1.2×10^6	1.38, 1.72	−0.44 ($n = 2$)
	bare SiO_2	2.8×10^{-4} (n)	25	7.2×10^5		−1.15 ($n = 2$)
4	PS−SiO_2	1.6×10^{-4} (p)	−34	6×10^5	1.04, 1.27	−0.45 ($n = 2$)
	bare SiO_2	2.7×10^{-5} (p)	−21	2.2×10^4		−1.13 ($n = 2$)

[a] $n = 2$ means that the reduction process is a two-electron process.

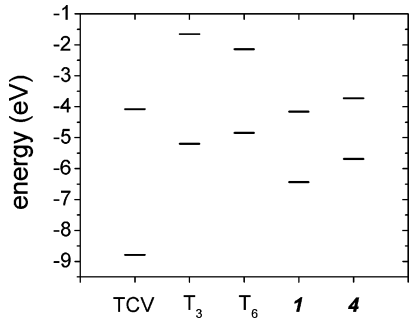

Figure 2. DFT-B3LYP/6-31G(d,p)-calculated HOMO and LUMO energies of TCV, T_3, T_6, **1**, and **4**.

electronic coupling between these two units is increased, enhancing the delocalization of the molecular orbital.

In conclusion, in **4**, HOMO is localized mostly in the oligothiophene unit, while the LUMO is on the TCV group, as expected from the analysis of the electronic structure of the separate units. In the case of **1**, the smaller separation of the TCV leads delocalization of both molecular orbitals due to electronic coupling between the two TCV groups.

From the transport point of view, the localization of the electronic density on the TCV groups in **4** suggests that these groups could act as traps for electrons injected in the conduction band. The delocalization of the HOMO, on the other hand, suggests that holes will be more mobile. These results are in agreement with the experimental mobilities (holes and electrons) measured for **4**, which will be described in section 3.E.

3.D. Thin Film Microstructure. The thin films of **1** were deposited on bare SiO_2 and $C_{16}-Al_2O_3$ substrates with the substrate temperature held at 110 °C and all of these films were crystalline as shown in Figure 4a. The primary *d* spacings for the films on $C_{16}-Al_2O_3$ and bare SiO_2 were 18.77 and 19.58 Å, respectively. There are 3 orders of diffraction for films grown on $C_{16}-Al_2O_3$ substrates and 2 orders on bare SiO_2. The film diffraction pattern corresponds well with powder diffraction pattern, which is shown in the inset of Figure 4a. Figure 5a shows the AFM topographical image of **1** on $C_{16}-Al_2O_3$ with a step height of 21 ± 1 Å, which is consistent with the XRD data and calculated molecular length of 19.5 Å. We infer that the molecules are oriented with their long axes approximately perpendicular to the substrate.

The thin films of **2** were deposited on bare SiO_2 and HMDS−SiO_2 substrates with the substrate temperature held at 106 °C and all of these films were also highly crystalline as shown in Figure 4b. The primary *d* spacings were 19.28 Å for films on bare SiO_2 and 19.31 Å for films on HMDS−SiO_2, which are consistent with a calculated molecular length of 19.25 Å. In addition to these peaks, a second set of peaks is present, corresponding to primary *d* spacings of 13.37 and 13.49 Å for films on bare SiO_2 and HMDS−SiO_2, respectively. While a peak corresponding to a 19.25 Å *d* spacing is apparent in the powder pattern (see inset, $2\theta = 4.7°$), we attribute the 13.37 Å peak to a thin film phase. The AFM topographic image of the film grown on bare SiO_2 is shown in Figure 5b. Long rectangular grains are evident that appear to grow over thin plates next to the substrate, suggesting the presence of a second phase.

The thin films of **3** were deposited on bare SiO_2 and HMDS−SiO_2 substrates with substrate temperature held at 103 °C and all of these films were crystalline as shown in Figure 4c. The

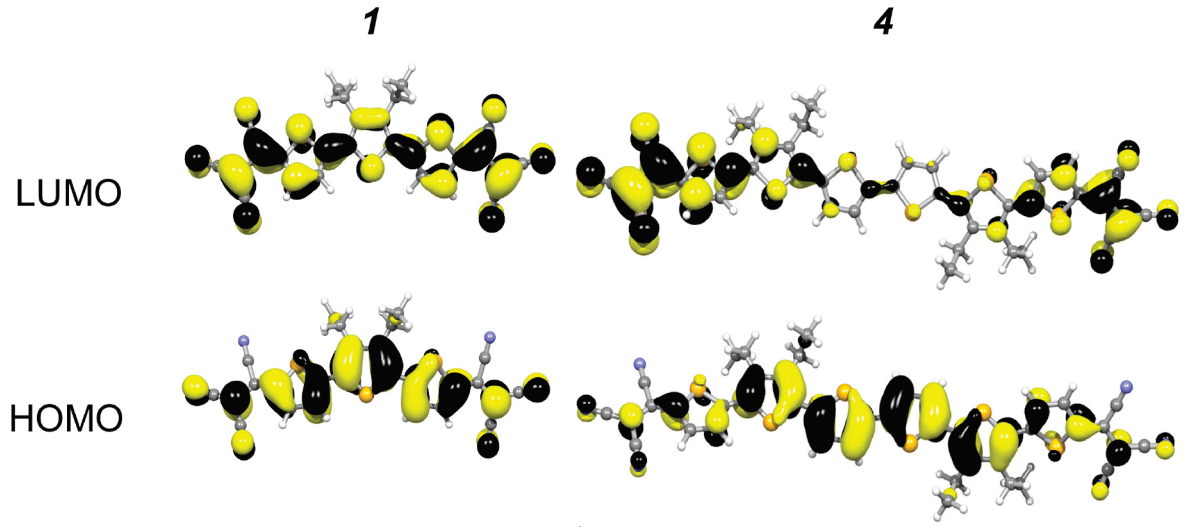

Figure 3. DFT-B3LYP/6-31G(d,p)-calculated HOMO and LUMO wave functions of **1** and **4**.

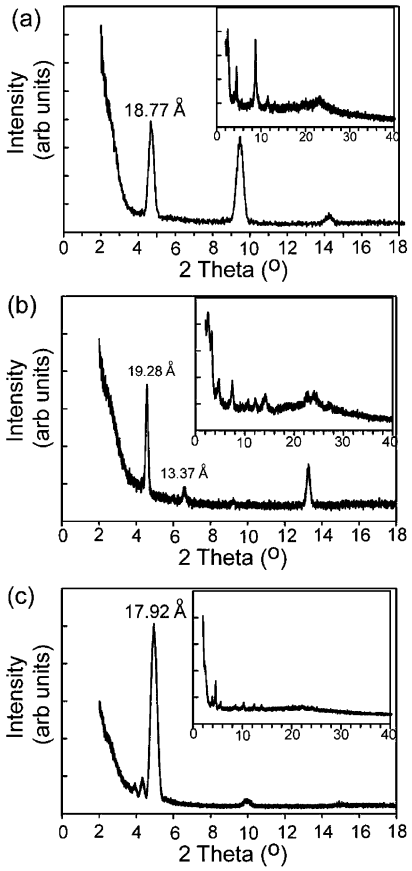

Figure 4. Thin film X-ray diffraction pattern for a 350 Å film of (a) **1** on $C_{16}-Al_2O_3$ grown at $T_s = 110$ °C, (b) **2** on bare SiO_2 substrate at $T_s = 106$ °C, and (c) **3** on bare SiO_2 substrate at $T_s = 103$ °C. Insets show powder diffraction patterns corresponding to each compound. The films are highly crystalline and *d* spacings at the primary peaks indicate it is highly possible that the π-stacking occurs in the thin films with its direction parallel to the substrates.

primary *d* spacings of these films were 17.92 Å for bare SiO_2 substrates and 18.44 Å for HMDS$-SiO_2$ substrates. There were 3 orders of diffraction for the film grown on bare SiO_2 substrates and only 1 for HMDS$-SiO_2$ substrates, indicating better ordering on SiO_2. Figure 5c showed an AFM topographic image with terraced grains with step heights of 17 ± 1 Å, consistent with the XRD data. The calculated molecular length is 23.5 Å, indicating the molecule may stand on the substrate surface with a 50° tilting angle.

Thin films of **4** were deposited on bare SiO_2 and PS$-SiO_2$ substrates. We were not able to obtain XRD peaks for films of **4** regardless of the substrate temperature during deposition. We infer that films of **4** are amorphous.

The single-crystal structure of **1** has been reported previously[23] and reveals that **1** forms π-stacks, although the single-crystal structure was obtained from samples with included solvent molecules. Based on the comparison of the XRD and AFM data and the calculated molecular length, we believe that π-stacking occurs in thin films of **1** and that the π-stacking direction is parallel to the substrate which should facilitate transport. This proposed structure is similar to what we reported for DCMT.[20]

3.E. Room-Temperature Electrical Characterization. TFTs of all four compounds fabricated with Ag top contacts were characterized in a vacuum at room temperature. $I_D - V_D$ and $I_D - V_G$ sweep curves of **1** are shown in Figure 6. Importantly, the device turns on with positive V_G, indicating n-channel

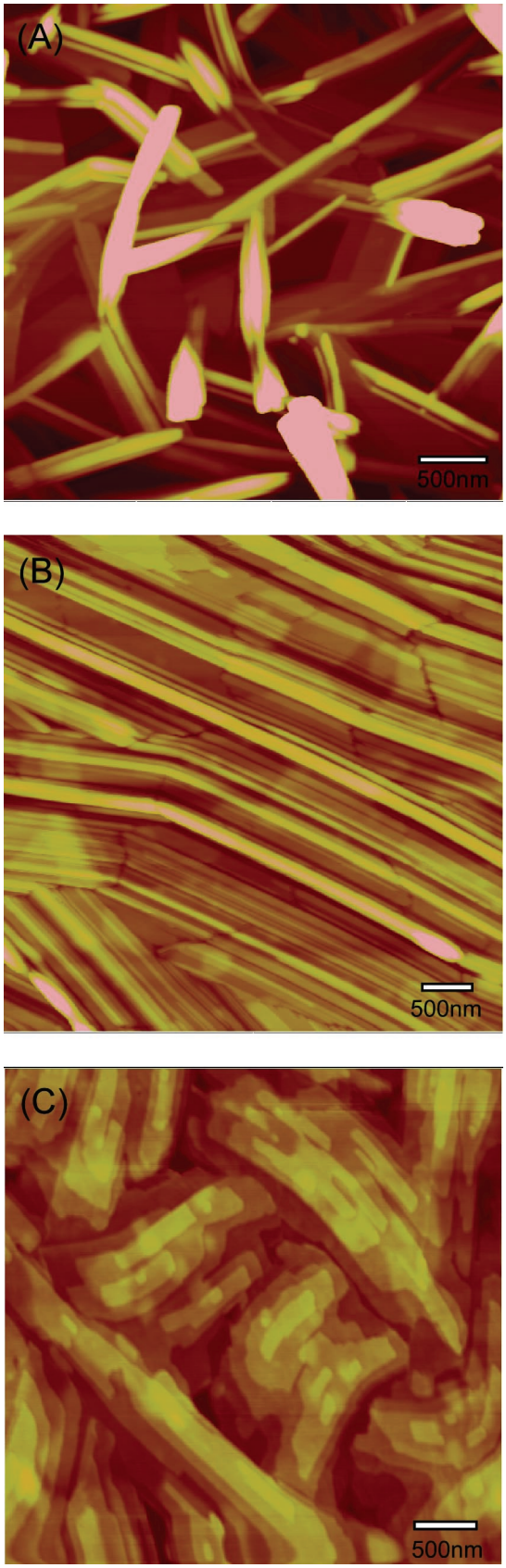

Figure 5. AFM topographic images of a 350 Å film of (a) **1** on $C_{16}-Al_2O_3$ substrate, (b) **2** on bare SiO_2 substrate, and (c) **3** on bare SiO_2 substrate.

(electron-transporting) behavior. **2** and **3** had similar n-channel behavior. The device performance is summarized in Table 1 together with electrochemical data. Thin films of **1** grown on

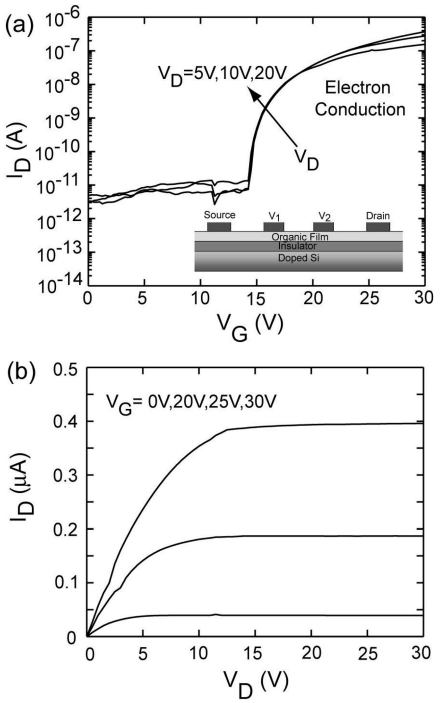

Figure 6. (a) Transfer and (b) output characteristics of thin film transistors based on films of **1** grown on $C_{16}-Al_2O_3$ at $T_s = 110$ °C, showing n-channel behavior. **2**, **3**, and **4** showed similar characteristics. The inset in (a) shows the device scheme.

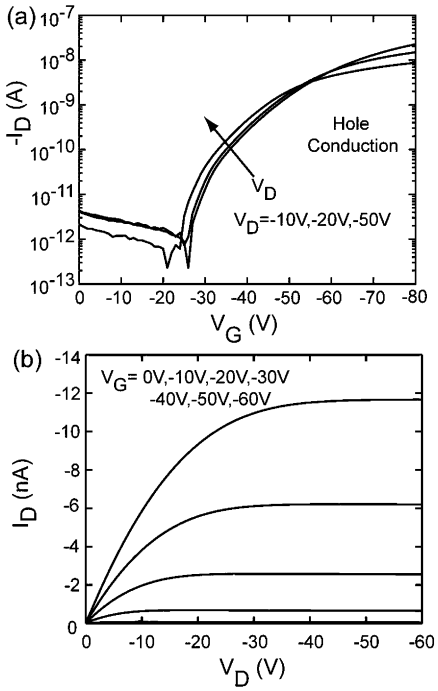

Figure 7. (a) Transfer and (b) output characteristics of thin film transistors based on films of **4** grown on $PS-SiO_2$ at room temperature, showing p-channel behavior.

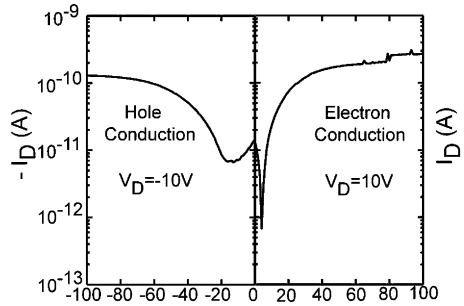

Figure 8. Ambipolar transport characteristics of thin film transistors based on films of **4** grown on $PS-SiO_2$ at a substrate temperature of 66 °C.

$C_{16}-Al_2O_3$ showed the highest contact-corrected linear electron mobility (0.02 $cm^2/V\cdot s$) and on/off current ratio (10^6). For all the compounds, the devices fabricated on hydrophobic substrates have better performance than those on hydrophilic substrates, which has been observed for other organic semiconductors.[40−43] There was no straightforward correlation between the improved electrical properties and AFM images and XRD patterns. A possible reason for improved performance is that the hydrophobic surface treatment decreased the carrier trap density at the organic/insulator interface.

Thin films of **4** grown at room temperature exhibited p-channel behavior (turned on with negative V_G) as shown in Figure 7, with a hole mobility of 1.1×10^{-4} $cm^2/V\cdot s$ and an on/off current ratio of 6×10^5. Ambipolar transport, i.e., both electron and hole conduction, as shown in Figure 8, was observed for thin films of **4** grown at elevated $PS-SiO_2$ substrate temperature, 66 °C, with a hole mobility of 7.9×10^{-8} $cm^2/V\cdot s$ and electron mobility of 2.1×10^{-7} $cm^2/V\cdot s$. Electron conduction dominated as the gate voltage was swept in the positive direction while hole conduction occurred as the gate voltage was swept in the negative direction.

3.E. Variable Temperature Measurements. Variable temperature measurements were done between 145 and 315 K on transistors of **1** on $C_{16}-Al_2O_3$ using a 4-probe geometry to correct for contact resistance. The temperature-dependent charge carrier transport behavior can be explained via the multiple trapping and release (MTR) model like many other organic semiconductors.[44−47] The evolution of onset voltage as a function of temperature is shown in Figure 9a. The MTR model suggests that the lower the temperature, the more charges are trapped and a larger gate voltage is required to induce enough charges to turn the devices on. From this description, the onset voltages are only affected by deep traps, whose density can be estimated by $\Delta V_0 C_i$. The estimated deep traps density is 2.7×10^{12} traps/cm^2. Figure 9b shows temperature dependence of the contact-corrected linear mobility for **1** on $C_{16}-Al_2O_3$. This temperature dependence can also be explained via the MTR model, which proposes that the mobility can be described by an Arrhenius equation,

$$\mu_{\text{eff}} \approx \mu_0 \exp\left(\frac{-E_A}{kT}\right) \tag{2}$$

where μ_{eff} is the effective mobility, μ_0 is an intrinsic mobility, and E_A is the activation energy. From Figure 9b, the activation energy is calculated to be about 88 meV. As shown in Figure 9c, the modified transconductance (g_M) was used to investigate the gate voltage dependence of the transport activation energy.

$$g_M = \frac{d\left(\frac{I_D}{V_{12}}\right)}{dV_G} \tag{3}$$

It is clear from Figure 9c that the activation energy decreases as gate voltage increases, which indicates that the Fermi level is moving through traps distributed in energy (near the LUMO) instead of single energy trap level.

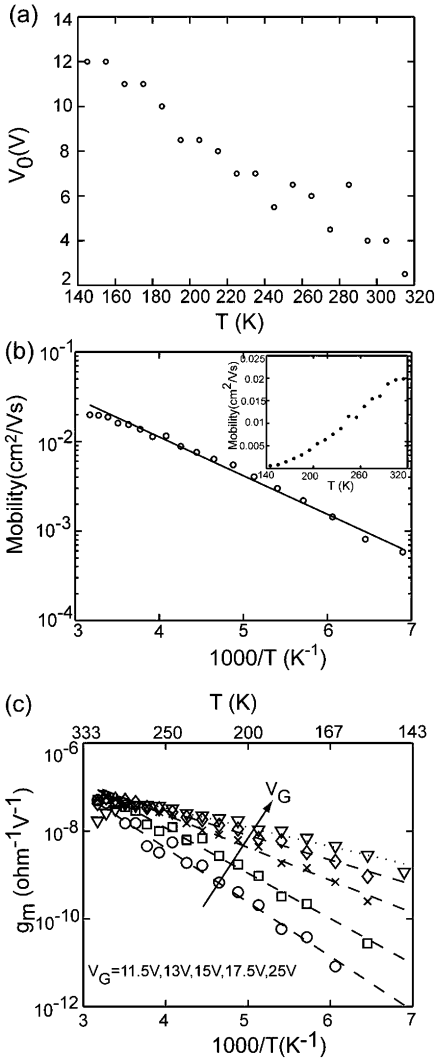

Figure 9. Variable temperature measurements on thin film transistors based on films of **1.** (a) Evolution of onset voltage as a function of temperature at $V_D = 5$ V. (b) Temperature dependence of contact-corrected linear mobility at $V_D = 5$ V, fitted via Arrhenius equation. The inset shows the temperature dependence of mobility without any fitting. (c) Temperature and gate voltage dependence of transconductance in a linear regime $V_D = 5$ V. The activation energy, i.e., the slope of log(transconductance) vs temperature, decreases as the gate voltage increases.

4. Conclusion

In summary, organic thin film field effect transistors were fabricated using four TCV-capped oligothiophene compounds. Reasonable n-channel transport behavior was obtained from oligomers **1**, **2**, and **3**, consistent with electrochemical data that showed these compounds undergo facile reduction. Variable temperature measurements on thin film devices of **1** suggest that the transport is dominated by traps distributed in energy. The redox properties and thin film transistor performance of **1**−**4** depend on the number of thiophene rings. In particular, inversion of the majority charge carrier type was observed when the number of oligothiophene rings was increased to 6. These results reinforce the general findings reported in the literature that substitution of "p-type" organic semiconductor molecules with electron-withdrawing groups provides a convenient strategy for realizing "n-type" materials.

Acknowledgment. This work was primarily supported by the NSF Materials Research Science and Engineering Center Program (DMR-0212302).

References and Notes

(1) Katz, H. E., Dodabalapur, A., Bao, Z., Eds. *Handbook of Oligo- and Polythiophenes*; Wiley-VCH: Weinheim, Germany, 1999; p 459.
(2) Locklin, J.; Li, D.; Mannsfeld, S. C. B.; Borkent, E.-J.; Meng, H.; Advincula, R.; Bao, Z. *Chem. Mater.* **2005**, *17*, 3366−3374.
(3) Facchetti, A.; Letizia, J.; Yoon, M.-H.; Mushrush, M.; Katz, H. E.; Marks, T. J. *Chem. Mater.* **2004**, *16*, 4715−4727.
(4) Nenajdenko, V. G.; Sumerin, V. V.; Chernichenko, K. Y.; Balenkova, E. S. *Org. Lett.* **2004**, *6*, 3437−3439.
(5) Chang, P. C.; Lee, J.; Huang, D.; Subramanian, V.; Murphy, A. R.; Frechet, J. M. J. *Chem. Mater.* **2004**, *16*, 4783−4789.
(6) Johansson, E.; Larsson, S. *Synth. Met.* **2004**, *144*, 183−191.
(7) Ruiz Delgado, M. C.; Casado, J.; Hernandez, V.; Lopez Navarrete, J. T.; Fuhrmann, G.; Baeuerle, P. *J. Phys. Chem., B* **2004**, *108*, 3158−3167.
(8) Meinardi, F.; Cerminara, M.; Blumstengel, S.; Sassella, A.; Borghesi, A.; Tubino, R. *Phys. Rev. B* **2003**, *67*, 184205/184201−184205/184206.
(9) Facchetti, A.; Mushrush, M.; Katz, H. E.; Marks, T. J. *Adv. Mater.* **2003**, *15*, 33−38.
(10) Meng, H.; Zheng, J.; Lovinger, A. J.; Wang, B.-C.; Van Patten, P. G.; Bao, Z. *Chem. Mater.* **2003**, *15*, 1778−1787.
(11) Deman, A. L.; Tardy, J.; Nicolas, Y.; Blanchard, P.; Roncali, J. *Synth. Met.* **2004**, *146*, 365−371.
(12) Halik, M.; Klauk, H.; Zschieschang, U.; Schmid, G.; Ponomarenko, S.; Kirchmeyer, S.; Weber, W. *Adv. Mater.* **2003**, *15*, 917−922.
(13) Fichou, D. *J. Mater. Chem.* **2000**, *10*, 571−588.
(14) Mohapatra, S.; Holmes, B. T.; Newman, C. R.; Prendergast, C. F.; Frisbie, C. D.; Ward, M. D. *Adv. Funct. Mater.* **2004**, *14*, 605−609.
(15) Newman, C. R.; Frisbie, C. D.; da Silva Filho, D. A.; Brédas, J.-L.; Ewbank, P. C.; Mann, K. R. *Chem. Mater.* **2004**, *16*, 4436−4451.
(16) Facchetti, A.; Yoon, M.-H.; Katz, H. E.; Mushrush, M.; Marks, T. J. *Mater. Res. Soc. Symp. Proc.* **2003**, *771*, 397−402.
(17) Facchetti, A.; Yoon, M.-H.; Stern, C. L.; Hutchison, G. R.; Ratner, M. A.; Marks, T. J. *J. Am. Chem. Soc.* **2004**, *126*, 13480−13501.
(18) Facchetti, A.; Yoon, M.-H.; Stern, C. L.; Katz, H. E.; Marks, T. J. *Angew. Chem., Int. Ed.* **2003**, *42*, 3900−3903.
(19) Yoon, M.-H.; DiBenedetto, S. A.; Facchetti, A.; Marks, T. J. *J. Am. Chem. Soc.* **2005**, *127*, 1348−1349.
(20) Chesterfield, R. J.; Newman, C. R.; Pappenfus, T. M.; Ewbank, P. C.; Haukaas, M. H.; Mann, K. R.; Miller, L. L.; Frisbie, C. D. *Adv. Mater.* **2003**, *15*, 1278−1282.
(21) Pappenfus, T. M.; Chesterfield, R. J.; Frisbie, C. D.; Mann, K. R.; Casado, J.; Raff, J. D.; Miller, L. L. *J. Am. Chem. Soc.* **2002**, *124*, 4184−4185.
(22) Bader, M. M.; Custelcean, R.; Ward, M. D. *Chem. Mater.* **2003**, *15*, 616−618.
(23) Pappenfus, T. M.; Burand, M. W.; Janzen, D. E.; Mann, K. R. *Org. Lett.* **2003**, *5*, 1535−1538.
(24) Barclay, T. M.; Cordes, A. W.; MacKinnon, C. D.; Oakley, R. T.; Reed, R. W. *Chem. Mater.* **1997**, *9*, 981−990.
(25) Janzen, D. E.; Burand, M. W.; Ewbank, P. C.; Pappenfus, T. M.; Higuchi, H.; da Silva Filho, D. A.; Young, V. G.; Brédas, J.-L.; Mann, K. R. *J. Am. Chem. Soc.* **2004**, *126*, 15295−15308.
(26) Graf, D. D.; Duan, R. G.; Campbell, J. P.; Miller, L. L.; Mann, K. R. *J. Am. Chem. Soc.* **1997**, *119*, 5888−5899.
(27) Becke, A. D. *Phys. Rev. A* **1988**, *38*, 3098−3100.
(28) Becke, A. D. *J. Chem. Phys.* **1993**, *98*, 1372−1377.
(29) Lee, C.; Yang, W.; Parr, R. G. *Phys. Rev. B* **1988**, *37*, 785−789.
(30) Frisch, M. J.; Trucks, G. W.; Schlegel, H. B.; Scuseria, G. E.; Robb, M. A.; Cheeseman, J. R.; Montgomery, J. A., Jr.; Vreven, T.; Kudin, K. N.; Burant, J. C.; Millam, J. M.; Iyengar, S. S.; Tomasi, J.; Barone, V.; Mennucci, B.; Cossi, M.; Scalmani, G.; Rega, N.; Petersson, G. A.; Nakatsuji, H.; Hada, M.; Ehara, M.; Toyota, K.; Fukuda, R.; Hasegawa, J.; Ishida, M.; Nakajima, T.; Honda, Y.; Kitao, O.; Nakai, H.; Klene, M.; Li, X.; Knox, J. E.; Hratchian, H. P.; Cross, J. B.; Adamo, C.; Jaramillo, J.; Gomperts, R.; Stratmann, R. E.; Yazyev, O.; Austin, A. J.; Cammi, R.; Pomelli, C.; Ochterski, J. W.; Ayala, P. Y.; Morokuma, K.; Voth, G. A.; Salvador, P.; Dannenberg, J. J.; Zakrzewski, V. G.; Dapprich, S.; Daniels, A. D.; Strain, M. C.; Farkas, O.; Malick, D. K.; Rabuck, A. D.; Raghavachari, K.; Foresman, J. B.; Ortiz, J. V.; Cui, Q.; Baboul, A. G.; Clifford, S.; Cioslowski, J.; Stefanov, B. B.; Liu, G.; Liashenko, A.; Piskorz, P.; Komaromi, I.; Martin, R. L.; Fox, D. J.; Keith, T.; Al-Laham, M. A.; Peng, C. Y.; Nanayakkara, A.; Challacombe, M.; Gill, P. M. W.; Johnson, B. G.; Chen, W.; Wong, M. W.; Gonzalez, C.; Pople, J. A. *Gaussian 03 (Revision B.01)*; Gaussian, Inc.: Pittsburgh, PA, 2003.
(31) Ditchfield, R.; Hehre, W. J.; Pople, J. A. *J. Chem. Phys.* **1971** *54*, 724−728.
(32) Hehre, W. J.; Ditchfield, R.; Pople, J. A. *J. Chem. Phys.* **1972**, *56*, 2257−2261.
(33) Harihara, P. C.; Pople, J. A. *Mol. Phys.* **1974**, *27*, 209−214.
(34) Gordon, M. S. *Chem. Phys. Lett.* **1980**, *76*, 163−168.

(35) Hariharam, P. C.; Pople, J. A. *Theor. Chim. Acta* **1973**, *28*, 213−222.

(36) Cai, C.; Liakatas, I.; Wong, M.-S.; Boesch, M.; Bosshard, C.; Guenter, P.; Concilio, S.; Tirelli, N.; Suter, U. W. *Org. Lett.* **1999**, *1*, 1847−1849.

(37) Wang, Y.-K.; Shu, C.-F.; Breitung, E. M.; McMahon, R. J. *J. Mater. Chem.* **1999**, *9*, 1449−1452.

(38) Bu, X. R.; Li, H.; Van Derveer, D.; Mintz, E. A. *Tetrahedron Lett.* **1996**, *37*, 7331−7334.

(39) Casado, J.; Ruiz Delgado, M. C.; Rey Merchán, M. C.; Hernández, V.; Lǒpetz Navarrete, J. T.; Pappenfus, T. M.; Williams, N.; Stregner, W. J.; Johnson, J. C.; Edlund, B. A.; Janzen, D. E.; Mann, K. R.; Orduna, J.; Villacampa, B. *Chem. Eur. J.* **2006**, in press.

(40) Sirringhaus, H.; Tessler, N.; Friend, R. H. *Science* **1998**, *280*, 1741−1744.

(41) Shtein, M.; Mapel, J.; Benziger, J. B.; Forrest, S. R. *Appl. Phys. Lett.* **2002**, *81*, 268−270.

(42) Sirringhaus, H.; Brown, P. J.; Friend, R. H.; Nielsen, M. M.; Bechgaard, K.; Langeveld-Voss, B. M. W.; Spiering, A. J. H.; Janssen, R. A. J.; Meijer, E. W.; Herwig, P.; De Leeuw, D. M. *Nature* **1999**, *401*, 685−688.

(43) Salleo, A.; Chabinyc, M. L.; Yang, M. S.; Street, R. A. *Appl. Phys. Lett.* **2002**, *81*, 4383−4385.

(44) Chesterfield, R. J.; McKeen, J. C.; Newman, C. R.; Frisbie, C. D.; Ewbank, P. C.; Mann, K. R.; Miller, L. L. *J. Appl. Phys.* **2004**, *95*, 6396−6405.

(45) Chesterfield, R. J.; McKeen, J. C.; Newman, C. R.; Ewbank, P. C.; da Silva Filho, D. A.; Brédas, J.-L.; Miller, L. L.; Mann, K. R.; Frisbie, C. D. *J. Phys. Chem., B* **2004**, *108*, 19281−19292.

(46) Horowitz, G.; Hajlaoui, M. E.; Hajlaoui, R. *J. Appl. Phys.* **2000**, *87*, 4456−4463.

(47) Horowitz, G.; Hajlaoui, R.; Delannoy, P. *J. Phys. III* **1995**, *5*, 355−371.